JACS
JOURNAL OF THE AMERICAN CHEMICAL SOCIETY
pubs.acs.org/JACS

Article

Interactions of Polar and Nonpolar Groups of Alcohols in Zeolite Pores

Ruixue Zhao,* Sungmin Kim,* Mal-Soon Lee,* Benjamin A. Jackson, Fuli Deng, Xiaomai Chen, Cong Zhou, Konstantin Khivantsev, Yue Liu, Vassiliki-Alexandra Glezakou, Roger Rousseau, and Johannes A. Lercher*

Cite This: J. Am. Chem. Soc. 2025, 147, 26049−26059

Read Online

ACCESS | Metrics & More | Article Recommendations | Supporting Information

ABSTRACT: Understanding the quantitative interactions among zeolite pore walls, Brønsted acid sites, and molecules with both polar and nonpolar regions is essential for scoping out the potential of zeolites as sorbents and catalysts. Purely siliceous zeolites (**MFI** and **Beta** in the present study) are hydrophobic, whereas those containing aluminum are considered hydrophilic, preferentially adsorbing organic molecules even in aqueous environments. To characterize these interactions, we use primary alcohols of increasing molecular weight, quantifying their specific interactions in the confined pore space of the alkyl (CH_x) and OH groups. Three types of interactions were identified: (i) alkyl CH_x groups interacting with the zeolite pore walls (approximately 10 kJ mol^{-1} per carbon), (ii) alcohol OH groups interacting with the pore walls (30−35 kJ mol^{-1}), and (iii) alcohol OH groups interacting with Brønsted acid sites (37 kJ mol^{-1}). All three interactions were well mirrored by computational simulations. The contribution of the alkyl CH_x groups was inferred from the incremental increase in sorption enthalpy with increasing molecular weight; the interaction strength of the OH groups was determined by extrapolating the global adsorption enthalpy of the alcohols to a hypothetical OH group without an alkyl group. This value was identical to the adsorption enthalpy of water. The experiments demonstrated that only water has an adsorption enthalpy on zeolite pore walls lower than its condensation enthalpy (30−35 kJ mol^{-1} vs 45 kJ mol^{-1}), limiting the concentration of water that can be adsorbed.

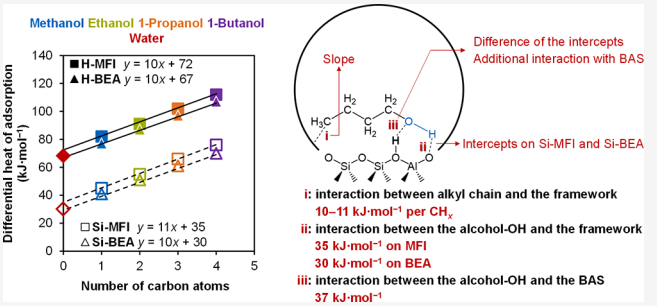

INTRODUCTION

Zeolites are tectosilicates frequently used as catalysts and sorbents; their well-defined pores comprise the three-dimensionally linked silica (and alumina if substituted) tetrahedra that vary in polarity depending on their chemical composition.[1−4] Colloquially, silica pore walls [$Si(OSi)_4$] are considered to be "hydrophobic", while acid−base sites, such as bridging Si−OH−Al, are considered to be "hydrophilic". The latter act as Brønsted acid sites (BAS) and are considered catalytically active binding sites interacting with reactants, intermediates, and products.

Weak interactions of nonpolar molecules in these pores rely predominantly on nondirected dispersion forces (dynamic interactions caused by polarity or dipoles induced by correlated electron movements). With alkanes, for example, the strength of these interactions is primarily determined by the size of the specific channel and the pore structure. On the other hand, strong interactions arise from directed hydrogen bonding or Coulomb interactions between polar functional groups of sorbed molecules.[5,6]

The adsorption of nonpolar molecules, such as short-chain alkanes, within zeolite pores has been well-investigated over the past few decades. With dispersion forces dominating, adsorption is intricately governed by factors such as the size of the alkane, the zeolite pore structure, and the acid−base sites present.[6−20] The differential heat of adsorption of alkanes increases with increasing alkane chain length, with each CH_x group contributing to the overall interaction: 10−12 kJ mol^{-1} for **MFI**,[7,21] 9 kJ mol^{-1} for **MOR**,[22] and 7 kJ mol^{-1} for **EMT**[7] and **FAU**.[7,22] The presence of BAS or metal cations at zeolite exchange positions imparts a heteropolar nature, introducing permanent electrostatic interactions.[6,22−25] We showed previously that the presence of BAS increases the adsorption enthalpy of alkanes by 10 kJ mol^{-1} for **MFI** and 6 kJ mol^{-1} for **FAU**. The difference has been tentatively attributed to differences in the acid strength.[7]

The adsorption of polar molecules such as water on zeolites containing BAS has been well-studied.[26−30] For example, in H-MFI, the first adsorbed water molecule interacts with the BAS

Received: June 3, 2025
Revised: June 26, 2025
Accepted: June 27, 2025
Published: July 12, 2025

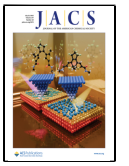

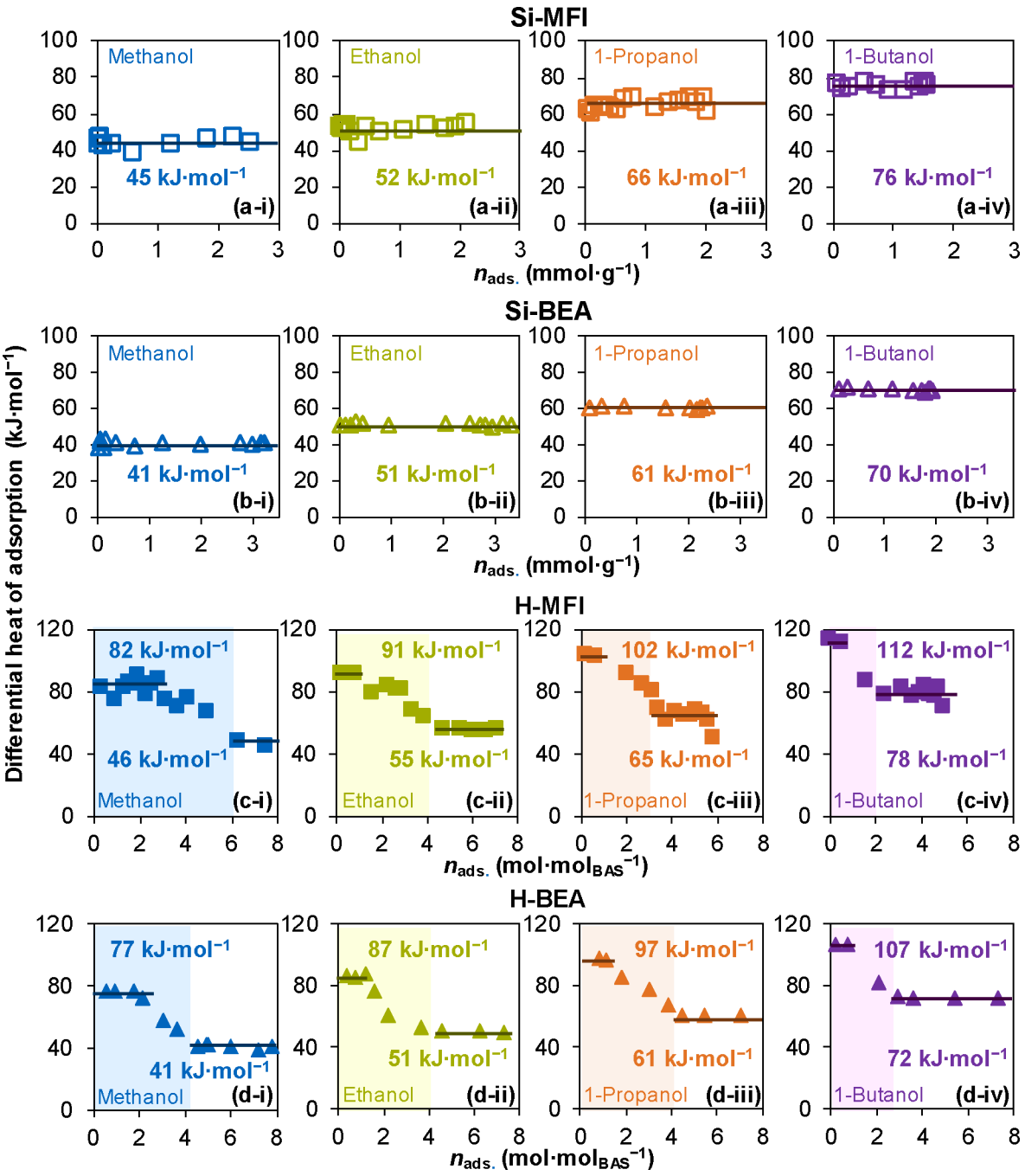

Figure 1. Heat of adsorption of C_1−C_4 primary alcohols on all samples. Differential heat of adsorption of C_1−C_4 primary alcohols as a function of alcohol uptake on (a-i)−(a-iv) Si-MFI and (b-i)−(b-iv) Si-BEA at 323 K. Differential heat of adsorption of C_1−C_4 primary alcohols as a function of adsorbed alcohol per BAS on (c-i)−(c-iv) H-MFI and (d-i)−(d-iv) H-BEA at 323 K.

through hydrogen bonding, while the proton remains on the Si−OH−Al group,[26,30] with an adsorption enthalpy of approximately 65 kJ mol^{-1}.[28] The heat of adsorption for the second water molecule (forming a dimer on BAS) increases to 85 kJ mol^{-1},[28] attributed to the proton transfer from the BAS forming a hydrated hydronium ion,[30,31] which has been characterized by high-resolution solid-state NMR spectroscopy.[30] Additional water molecules (up to approximately 8 per BAS) stabilized this cluster and gradually decreased the enthalpy of adsorption to 45 kJ mol^{-1},[28] comparable to the condensation enthalpy of water.[28,31] As an ensemble, all adsorbed water molecules form hydrated hydronium ions, closely associated with the negative charge on the zeolite framework. The concentration of such hydrated hydronium ions influences the binding of other molecules. Increasing concentration reduces the adsorption enthalpy while increasing the excess chemical potential of the sorbate at the initial state.[32,33] Hydronium ion concentration has been observed to cause a strong variation in the heat of sorption as well as an increase in the acid catalyzed reaction rates (e.g., alcohol dehydration) by lowering the excess chemical potential in the transition state; higher concentrations of hydronium ions lead to a decrease in the reaction rate due to rearrangement of the substrate and hydronium ion in the pore.[34,35]

https://doi.org/10.1021/jacs.5c09340
J. Am. Chem. Soc. 2025, 147, 26049−26059

As the alkyl group in alcohols is relatively nonpolar, while the hydroxyl group serves as a polar hydrogen-bonding site, the interactions between alcohols and zeolites encompass both dispersion forces and directed hydrogen bonding or protonation. Consequently, examining how alcohols interact within the pores of zeolites provides valuable insights into the distinct ways the silica framework and its discrete ion-exchange sites engage with the nonpolar and polar components of the sorbed molecules.

In the present work, we report the adsorption of short-chain (C_1−C_4) alcohols and water on **MFI** and **Beta** framework zeolites. In all samples, a linear correlation was observed between the heat of adsorption and the increasing carbon number, mirroring the enthalpy trends known from alkane adsorption.[7,21] Calorimetry and computational calculations quantified these interactions at the molecular level, providing insights into the role of the zeolite framework and acid sites in a reaction involving alcohol or water OH and alkyl groups. This understanding contributes to the design of catalysts with tailored catalytic activity and selectivity.

RESULTS AND DISCUSSION

C_1−C_4 Primary Alcohol Adsorption on Silicalite-1 (Si-MFI) and Siliceous Beta (Si-BEA). Figure 1a,b shows the differential heat of adsorption of C_1−C_4 primary alcohols on Si-MFI and Si-BEA zeolites as a function of alcohol uptake at 323 K. The adsorption of each alcohol on Si-MFI and Si-BEA shows the differential heat of adsorption to be invariant with respect to the amount of sorbed alcohol. Figure 2a plots the differential heat of adsorption as a function of the alcohol carbon number and shows the heat of alcohol adsorption on Si-MFI and Si-BEA increases linearly by 11 and 10 kJ mol^{-1} per CH_x group, respectively (from 45 and 41 kJ mol^{-1} for methanol to 76 and 70 kJ mol^{-1} for 1-butanol). These values are in line with the previous studies on alkane adsorption, where each CH_x group contributes 10−12 kJ mol^{-1} and 8−10 kJ mol^{-1} to the heat of adsorption on **MFI** and **Beta** framework, respectively.[11] The intercepts in Figure 2a allow quantifying the heat of adsorption contributed by interaction between the alcohol−OH group and the silica framework of the **MFI** and **Beta** channels, which are 35 kJ mol^{-1} (Si-MFI) and 30 kJ mol^{-1} (Si-BEA), respectively. The 5 kJ mol^{-1} higher value on Si-MFI compared to that on Si-BEA suggests a stronger interaction between the alcohol−OH and the **MFI** framework induced by the more constrained environment.

To deepen our understanding of how zeolite channels interact with sorbed alcohol molecules, we investigated the sorption of C_1−C_4 primary alcohols in Si-MFI using IR spectroscopy and compared these results to the spectra in the gas phase and those adsorbed on silica (Figure 3). Si-MFI was selected for this analysis due to its highly crystalline and highly defect-free structure, as evidenced by the very low intensities of silanol group-related bands in the IR spectra (Figure S1). This allows us to isolate interactions between alcohol molecules and the pore walls [$Si(OSi)_4$], excluding contributions from the silanol groups. Corresponding results for Si-BEA are provided in Supplementary Note 1. In the following discussion, the term "pore wall" refers specifically to the closed Si sites as [$Si(OSi)_4$].

In the gas-phase spectra (Figure 3a), the band at 3680 cm^{-1} is attributed to the OH stretching vibration of the unperturbed OH group of the alcohol. The bands between 2800 and 3000 cm^{-1} are attributed to the C−H vibrations of the alkyl groups.

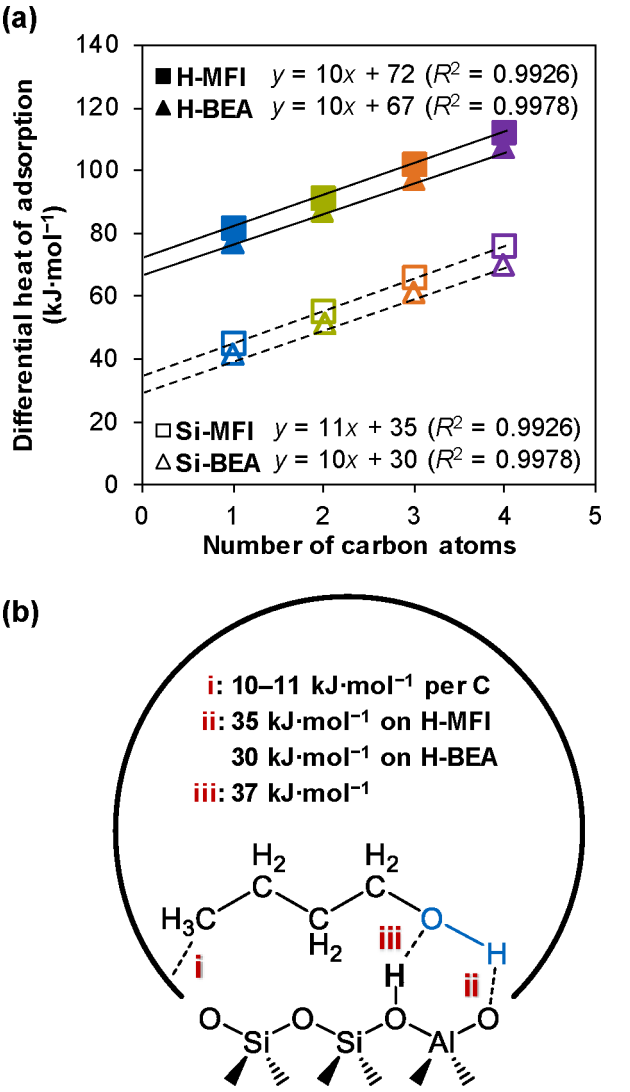

Figure 2. Differential heat of adsorption and energetic attribution of alcohol adsorption in zeolite. (a) Differential heat of adsorption of C_1−C_4 primary alcohols as a function of carbon atoms on Si-MFI (open square symbols), Si-BEA (open triangle symbols), H-MFI (solid square symbols), and H-BEA (solid triangle symbols) at 323 K. (The increment of the linear dependence on Si-MFI and Si-BEA indicates the interaction between each $-CH_2-$ (or $-CH_3$) group and the zeolite framework, and the intercept value indicates the interaction between the alcohol−OH group and the zeolite framework; the increment of the linear dependence on H-MFI and H-BEA indicates the interaction between each $-CH_2-$ (or $-CH_3$) group and the zeolite framework, and the intercept value indicates the interaction between the alcohol−OH group and the zeolite framework/BAS.) (b) Three kinds of interactions between a primary alcohol molecule (e.g., 1-butanol) and a BAS containing zeolite and their correlated contributions to the heat of adsorption.

In contrast, sorbed alcohols on SiO_2 (Figure 3b) do not exhibit a band for the free terminal OH. This absence is attributed to the interaction of the alcohol−OH group with the Si−OH groups, which not only leads to the negative band at 3742 cm^{-1} due to the perturbation of the Si−OH sites but also results in a band at 3320 cm^{-1}, indicating hydrogen bonding within clusters of molecules (Figure 3b).[36,37]

Upon alcohol adsorption on Si-MFI, three bands appeared at 3680, 3640, and 3510 cm^{-1} in the O−H vibration range. The first band (3680 cm^{-1}) is attributed to free alcohol−OH

https://doi.org/10.1021/jacs.5c09340
J. Am. Chem. Soc. 2025, 147, 26049−26059

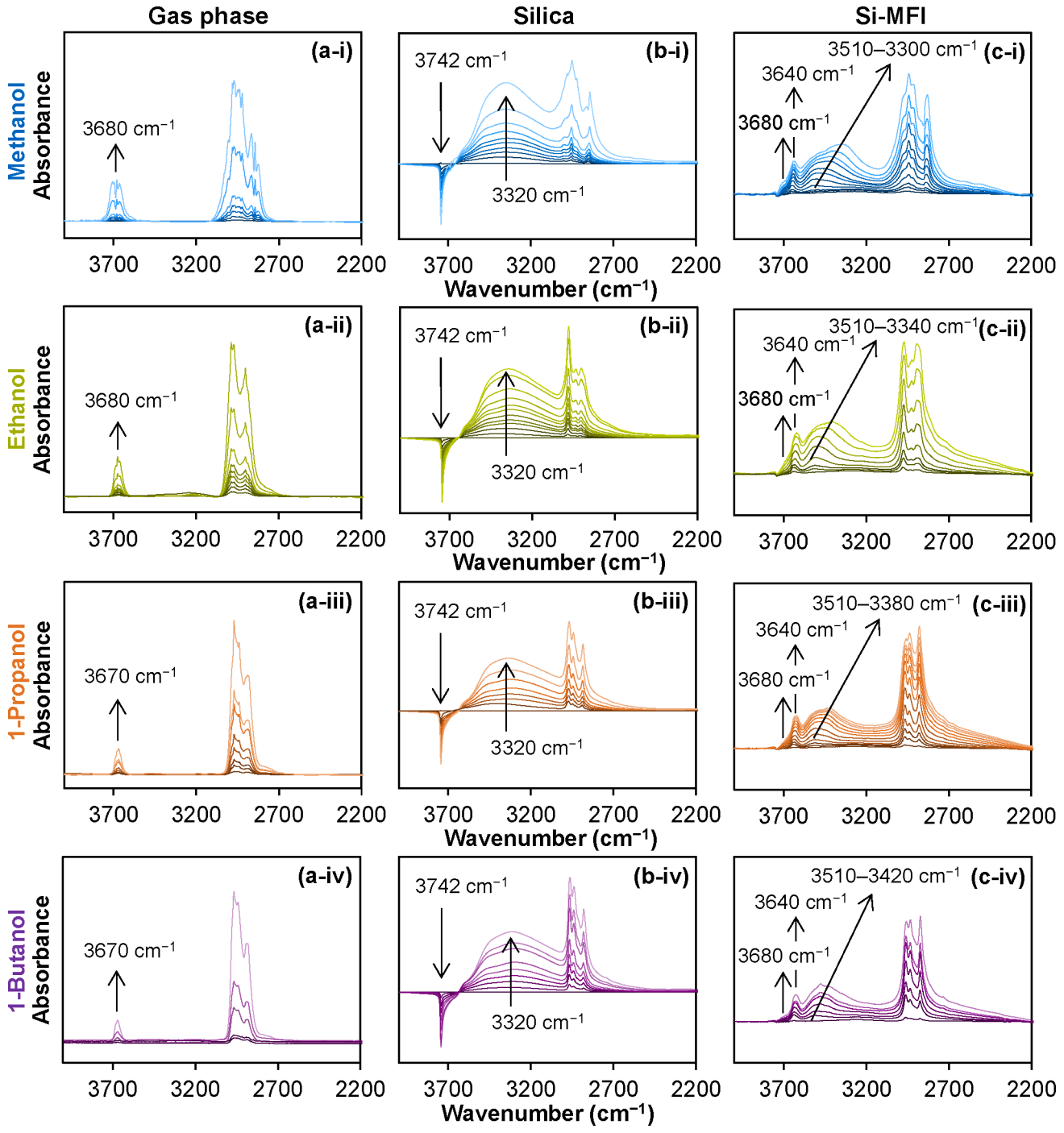

Figure 3. Infrared spectroscopy of C_1−C_4 primary alcohols. Infrared spectra of (a-i)−(a-iv) gas-phase C_1−C_4 primary alcohols, difference spectra of C_1−C_4 primary alcohols sorbed on (b-i)−(b-iv) silica (parent silica spectrum subtracted), and (c-i)−(c-iv) Si-MFI (parent Si-MFI spectrum subtracted). All spectra were recorded at 323 K under increasing pressure (1×10^{-3} to 20 mbar), with lighter colors representing higher pressures. Arrows indicate the trends in band changes.

groups of nonadsorbed molecules in the gas phase, which only appeared at high alcohol pressure. The second (3640 cm^{-1}) is assigned to alcohol molecules in the pores that do not interact with the pore walls. The shift of the free alcohol−OH group from 3680 cm^{-1} in the gas phase to 3640 cm^{-1} in Si-MFI is attributed to these weak interactions in the pore confinement.[38] When interacting with the pore walls, the vibrational band of the free terminal alcohol−OH group shifts from 3640 to 3510 cm^{-1}. This shift indicates a relatively strong interaction with the siliceous framework walls, likely enhanced by hydrogen bonding between alcohol molecules. As the alcohol concentration increased, the broad band gradually shifted to 3420−3300 cm^{-1}. Paralleling the development of larger alcohol clusters, it points to a strengthening of the interactions with the silicate pore walls as a result of the polarization of the molecules in the hydrogen-bonded clusters.

C_1−C_4 Primary Alcohol Adsorption on H-MFI and H-BEA. Figure 1c,d shows the differential heat of adsorption of C_1−C_4 primary alcohols on H-MFI and H-BEA zeolites as a function of adsorbed alcohol molecules per BAS. The

https://doi.org/10.1021/jacs.5c09340
J. Am. Chem. Soc. 2025, 147, 26049−26059

monomolecular adsorption ($n_{ads.} \leq 1$ $mol_{alcohol}$ mol_{BAS}^{-1}) results in a higher differential heat of adsorption, 82−112 kJ mol^{-1} and 77−107 kJ mol^{-1} for C_1−C_4 alcohols on H-MFI and H-BEA, respectively. The sorption enthalpy shows a linear relationship with the carbon number (Figure 2a), and the slope indicates that each CH_x group contributes 10 kJ mol^{-1}, in agreement with their contribution with siliceous zeolites (Si-MFI and Si-BEA). On the other hand, the intercepts were 72 and 67 kJ mol^{-1} for H-MFI and H-BEA, respectively. Comparing the 35 and 30 kJ mol^{-1} values measured for siliceous zeolites, we attribute the 37 kJ mol^{-1} enthalpy increase (both H-MFI and H-BEA) specifically to the interaction between the alcohol−OH group and the BAS. Incidentally, although both H-MFI and H-BEA contain some silanol groups, alcohol molecules in the monomolecular adsorption regime interact exclusively with the BAS, not with the silanol groups (Figure S3). Therefore, interactions between sorbed alcohol and silanol groups can be excluded when comparing the monomolecular adsorption stage.

After the first molecule adsorbs, the heat of adsorption of C_1−C_4 primary alcohols on H-MFI and H-BEA continuously decreases with each additional sorbed molecule ($n_{ads.} > 1$ $mol_{alcohol}$ mol_{BAS}^{-1}) converging to a value similar to the alcohol adsorption enthalpy on siliceous zeolites. Prior to convergence, H-MFI and H-BEA are always higher than the corresponding heat of adsorption for the siliceous zeolite. This suggests the existence of additional intermolecular interactions between the adsorbed alcohol molecules in the presence of the BAS, indicating the formation of alcohol clusters around the BAS due to the strengthening of hydrogen bonding by the protonation of the alcohol. The size of the cluster of different alcohols is discussed in Supplementary Note 3.

In summary, Figure 2b illustrates three distinct interactions between the alcohol molecule and the zeolite, i.e., (i) the alkyl chain interacts with the zeolite pore (approximately 10 kJ mol^{-1} per carbon atom); (ii) the alcohol−OH group interacts with the zeolite pore (35 kJ mol^{-1} in the **MFI** framework and 30 kJ mol^{-1} in the **Beta** framework); and (iii) the alcohol−OH group interacts with the BAS (37 kJ mol^{-1} in both **MFI** and **Beta** frameworks).

Relation between the Adsorption of the Alcohol−OH Group and Water. In our previous study, water adsorption on H-MFI showed that the first two sorbed water molecules interact strongly with the BAS, exhibiting an average heat of adsorption of approximately 71 kJ mol^{-1} (Figure 4a).[26−29,31] This value aligns with the intercept of the linear relationship between the differential heat of adsorption of C_1−C_4 alcohols and the number of carbon atoms (Figure 4c), representing the interaction between the alcohol−OH group and the zeolite framework/BAS (interactions ii and iii in Figure 2b). In consequence, the OH groups of water are concluded to interact with a strength similar to the OH group of alcohols (C_0OH). This is corroborated by the adsorption enthalpy of water on Si-MFI (33 kJ mol^{-1}) (Figure 4b), identical to the intercept of the extrapolated correlation of the adsorption enthalpies and the carbon number of the alcohol (Figure 4c).

It should be noted that Silicalite-1 (Si-MFI) is commonly regarded as "hydrophobic", i.e., only a small concentration of water can be adsorbed in the pores even in the presence of liquid water. The low concentration of water molecules in the pores stems from the fact that the enthalpy of condensation of water is higher (45 kJ mol^{-1}) than the heat of adsorption of the OH group (33 kJ mol^{-1}). This difference is due to the strong

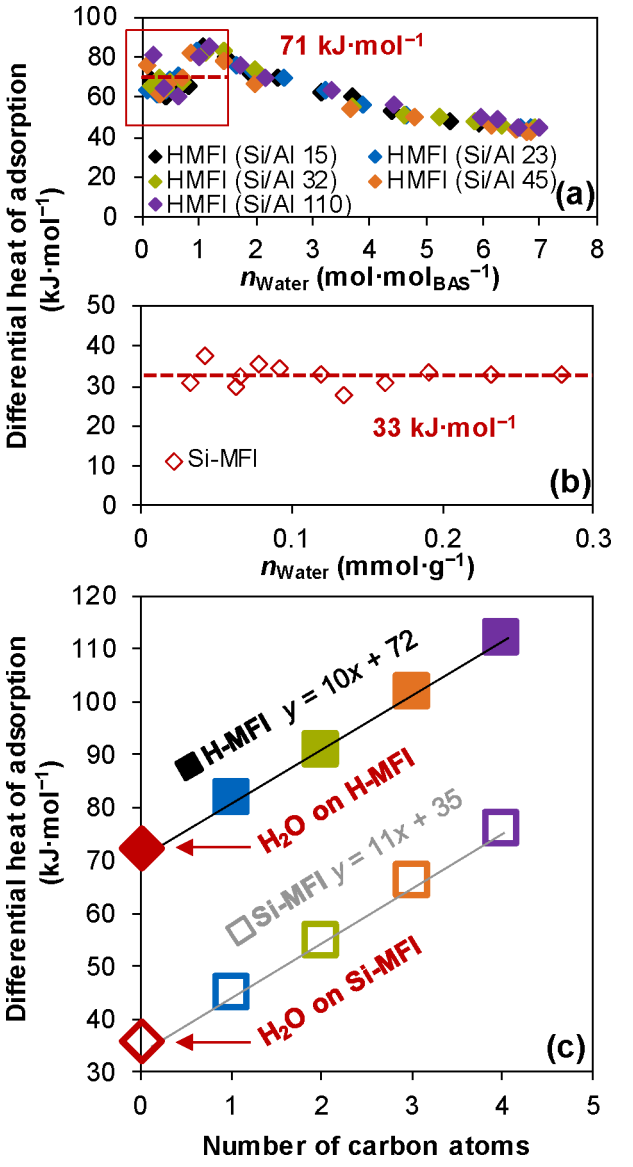

Figure 4. Differential heat of adsorption of water vs C_1−C_4 primary alcohols in MFI zeolites. Differential heat of adsorption of water as a function of adsorbed water on (a) H-MFI with different Si/Al ratios and (b) Si-MFI. (c) Differential heat of adsorption of water and C_1−C_4 primary alcohols as a function of carbon atoms on Si-MFI (open symbols) and H-MFI (solid symbols) at 298 K. (The heat of adsorption of water on H-MFI in (a) is adapted from ref 28. The heat of adsorption of water on H-MFI in (c) was calculated as the average value with $n_{Water} \leq 2$ mol mol_{BAS}^{-1}).

intermolecular hydrogen bonds in water (approximately 23.3 kJ mol^{-1}),[39] making it a unique sorbate compared to alcohols, whose heat of adsorption is generally higher than the condensation heat (Table S1). The more negative condensation enthalpy leads to very low concentrations of water in the pores of a perfect siliceous zeolite (OH group free) with the **MFI** structure. It is noticeable that the interaction between water and the "hydrophobic" pore is much stronger (33 kJ mol^{-1}) than the one of alkyl groups (10−11 kJ mol^{-1}). Thus, hydrogen bonding of the OH group of the alcohol (and of water) to the silica wall of the zeolite framework is stronger than the dispersive forces of the hydrocarbon groups. Clearly, the lower enthalpy gain with methanol and other alcohols upon condensation allows complete pore filling. It will be

https://doi.org/10.1021/jacs.5c09340
J. Am. Chem. Soc. 2025, 147, 26049−26059

interesting to explore how mixtures of water with alcohols partition between the pores and the liquid, allowing in turn to establish the thermodynamic states of the solution constituents with and without the constraints of a porous sorbent and a catalyst.

AIMD Simulations of Alcohol Adsorption on Si-MFI. To better understand the discrete interactions between alcohols and zeolites, we employed density functional theory (DFT) based on ab initio molecular dynamics (AIMD) simulations for the C_1-C_4 primary alcohols within the **MFI** frameworks. We generated trajectories for a single alcohol molecule within Si-MFI and H-MFI at 333 K. In the case of H-MFI, the simulation cell included only a single BAS.

Figure 5a shows the simulated adsorption enthalpy, $-\Delta H^\circ_{the.}$, of the alcohols in Si-MFI calculated by the quasi-harmonic approximation (QHA) method from the AIMD trajectories. $-\Delta H^\circ_{the.}$ increases linearly with increasing number of carbon atoms, the slope of which indicates that each CH_x contributes 9 kJ mol^{-1}, and the y-intercept provides the alcohol−OH interaction with the zeolite framework as 37 kJ mol^{-1}; the corresponding experimental values (Figure 2a) for Si-MFI are 11 and 35 kJ mol^{-1}. DFT simulations underestimate the CH_x binding by 2 kJ mol^{-1} and the OH interaction by the same value. Considering the typical accuracy of DFT calculations,[40,41] this is a very good agreement and strongly supports the validity of the structural analysis that follows. Figure 5b shows a linear correlation between experimental and theoretical enthalpy changes, with a slope of 0.86 and $R^2 = 0.98$, indicating that the theoretical results not only capture the overall trend but also closely match the adsorption enthalpy for the individual alcohols.

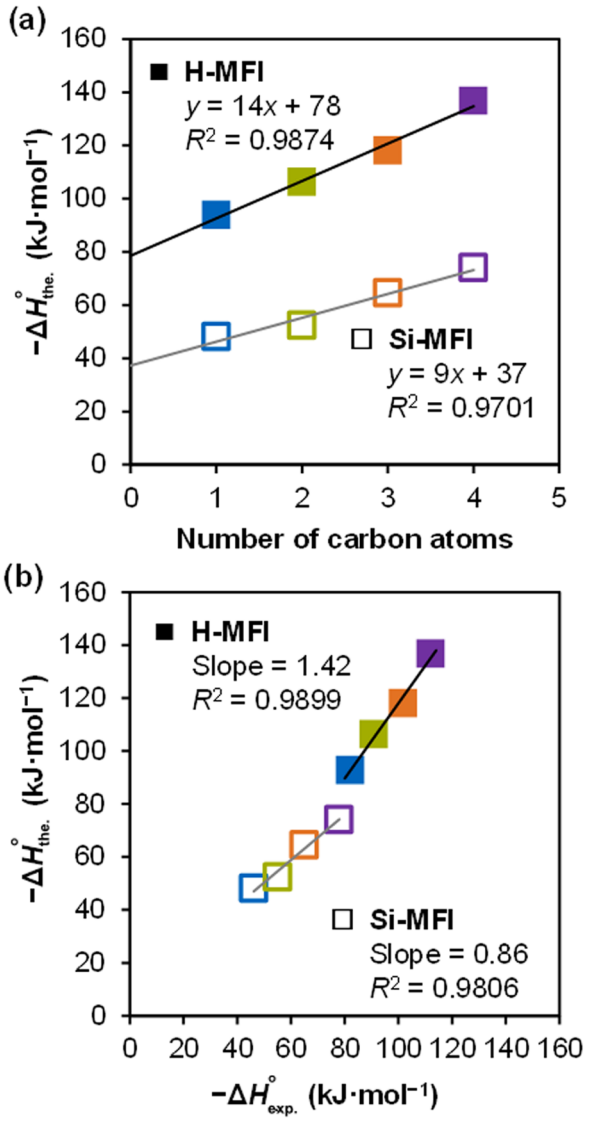

Figure 5. (a) Calculated standard enthalpy of adsorption, $-\Delta H^\circ_{ads}$, for C_1-C_4 primary alcohols in Si-MFI and H-MFI, and (b) comparison between calculated enthalpy, $-\Delta H^\circ_{the.}$, and the experimentally measured differential heat of adsorption, $-\Delta H^\circ_{exp}$.

We then computed the radial distribution function $g(R)$ using the AIMD trajectories, which provide the average distances between pairs of atoms. In Figure 6a, $g(R)$ is plotted for the distances between carbon atoms in the alcohol, C_A, and the oxygen and silicon atoms of the zeolite framework, O_Z and Si. The $g(R)$ values decrease with an increase in carbon numbers in the 3.0−5.5 Å distance range, while they increase in the 5.5−8.0 Å range (Figure 6a-ii). The free energy of the C_A-Si/O_Z interaction was estimated by calculating the potential of the mean force (PMF) as $V(R) = -RT\ln(g(R))$ (Figure 6a-iii). From this, we see that despite the apparent changes in $g(R)$ morphology the PMF experienced by each carbon atom is identical for C_1-C_4 (12.9 ± 0.37 kJ mol^{-1}). This observation explains the linear increase in $-\Delta H$ with an increasing number of carbons, consistent with experimental results.

Figure 6b depicts $g(R)$, showing distances for the alcohol hydrogen−oxygen (H_A-O_A) and the alcohol hydrogen to the zeolite framework oxygen (H_A-O_Z) for C_1-C_4. The H_A-O_A peak centered at about 1.0 Å is unchanged for C_1-C_4, showing that the carbon length has a negligible effect on the H_A-O_A interaction. The H_A-O_Z distances are similarly unaffected by the carbon length, with the shortest distance occurring at about 2.0 Å. Together, these two illustrate that the carbon chain length has no effect on both the intramolecular H_A-O_A and intermolecular H_A-O_Z interactions, explaining why the alcohol−OH group consistently contributes approximately 35 kJ mol^{-1} to the experimental adsorption enthalpy for C_1-C_4 alcohols.

AIMD Simulations of Alcohol Adsorption on H-MFI. As with Si-MFI, we observe a linear relationship between the calculated $-\Delta H$ and carbon number for C_1-C_4 primary alcohols in H-MFI. A linear fit indicates that each CH_x contributes 14 kJ mol^{-1} and the alcohol−OH contributes 78 kJ mol^{-1} to the enthalpy of adsorption (Figure 5a). Overall, the $-\Delta H^\circ_{the.}$ trend strongly agrees with the experimental differential heat of adsorption; the AIMD description of the alcohol−OH contribution to $\Delta H^\circ_{ads.}$ differs by only 6 kJ mol^{-1} and the CH_x component by 4 kJ mol^{-1}, relative to the experiment (Figure 2a). Comparing the experimental and theoretical adsorption enthalpies for C_1-C_4 (Figure 5b), we observe a strong linear relationship with a slope of 1.42 (R^2 = 0.9899), indicating a uniform overestimation of the calculated $\Delta H^\circ_{ads.}$. Initially, this suggests a discrepancy in the accuracy of the calculated $\Delta H^\circ_{ads.}$ in Si-MFI relative to H-MFI; however, it is crucial to emphasize that both exhibit remarkable agreement when considering the typical DFT error associated with describing adsorbate interactions using generalized gradient approximation (GGA) functionals.[40,41] Previous studies on zeolite adsorption of alkanes with a similar methodology have found errors on the order of 3−5 kJ mol^{-1}.[42]

https://doi.org/10.1021/jacs.5c09340
J. Am. Chem. Soc. 2025, 147, 26049−26059

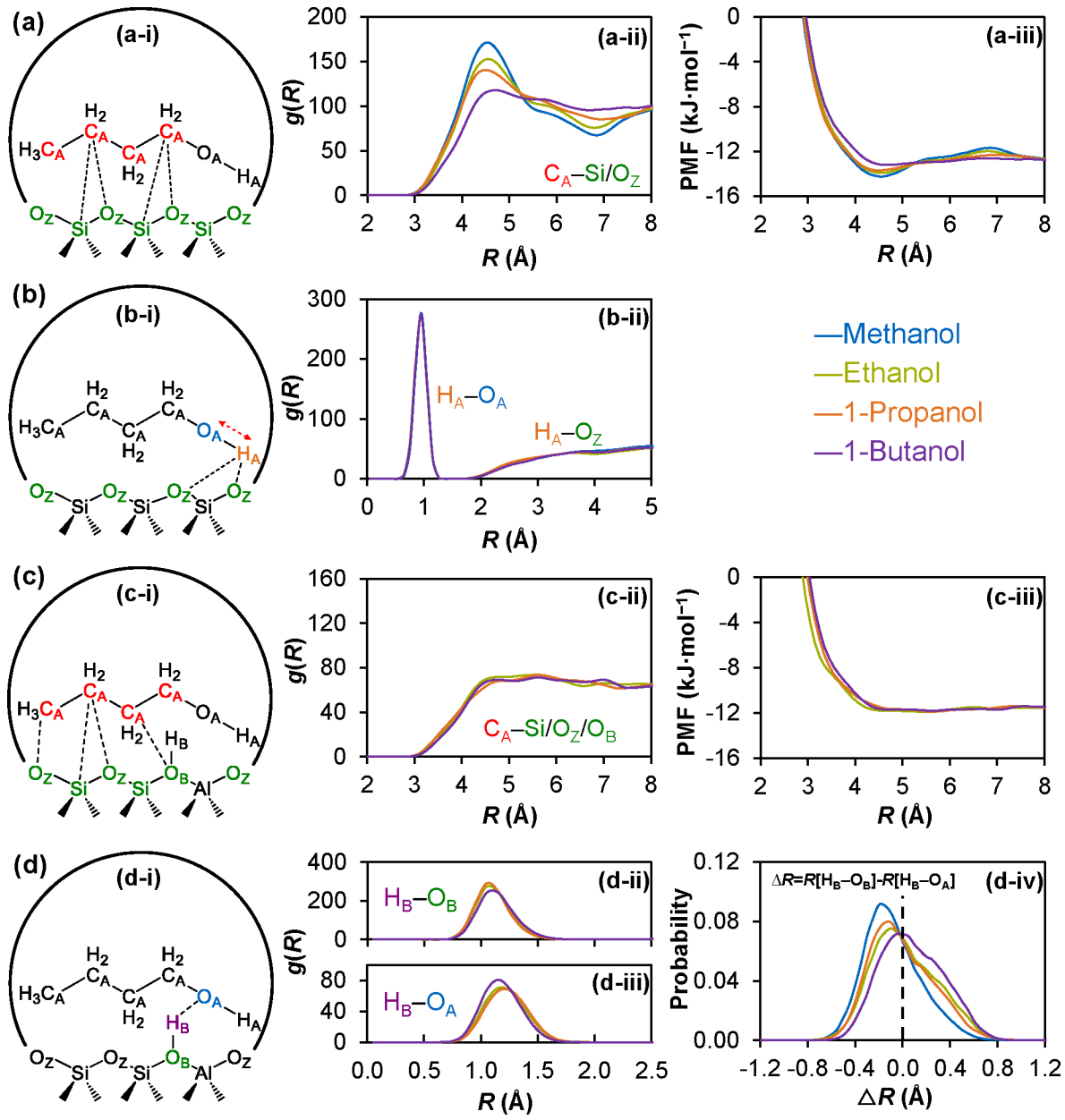

Figure 6. Interactions of C_1−C_4 primary alcohols in the MFI framework. In Si-MFI: (a-i) CH_x interactions of C_1−C_4 primary alcohols, (a-ii) radial distribution function, $g(R)$, for C_A, to Si and O_Z, and (a-iii) potential of mean force (PMF) calculated as $V(R) = -RT \ln(g(R))$, which is an estimate of the free energy of the average interaction between C_A and Si/O_Z. (b-i) OH interactions of C_1−C_4 primary alcohols in Si-MFI, (b-ii) $g(R)$ for H_A−O_A, as well as the $g(R)$ for H_A−O_Z. In H-MFI: (c-i) CH_x interactions of C_1−C_4 primary alcohols, (c-ii) $g(R)$ for C_A and Si/O_Z/O_B, and (c-iii) PMF of the average interaction between C_A and Si/O_Z/O_B. (d-i) OH interactions of C_1−C_4 primary alcohols in H-MFI, (b-ii) $g(R)$ for H_B−O_B, (b-iii) $g(R)$ for H_B−O_A for C_1−C_4, and (d-iv) probability distribution for the relative position of H_B between O_A and O_B. The difference in the H_B−O_B and O_A−H_B distances, ΔR, is calculated as $\Delta R = R[H_B - O_B] - R[H_B - O_A]$ at each time step (0.5 fs), followed by a histogram of ΔR values. Positive values indicate that the BAS proton is primarily on O_A and negative on O_B. (C_A, O_A, and H_A represent alcohol carbon, alcohol oxygen, and alcohol hydrogen, respectively; Si and O_Z represent framework silicon and oxygen, respectively; and H_B and O_B represent BAS proton and BAS oxygen, respectively).

For H-MFI, the presence of the BAS results in two distinct interactions of the alcohol carbons C_A with the zeolite oxygen, one for the zeolite framework, O_Z, and another for the oxygen of the acid site, O_B. Figure S6 plots the $g(R)$ and illustrates that there is a distinction in the C_A−O_B interaction for C_1−C_4, with each subsequent carbon added being further from O_B. However, this effect is insignificant compared to the more abundant C_A−O_Z interaction, which deviates little for C_1−C_4. This is clearly illustrated in Figure 6c-ii depicting the $g(R)$ for C_A to all atoms of the zeolite framework (Si, O_Z, and O_B), which shows strong morphological agreement for C_1−C_4. Also, the PMF of Figure 6c-iii shows each C_A experiences an identical force from the zeolite framework (11.7 ± 0.16 kJ mol^{-1}). Collectively, these observations elucidate why each CH_x equally contributes (experimental 9 kJ mol^{-1}) to the heat of adsorption.

Depicted in Figure 6d is the interaction of the BAS proton (H_B) with either the BAS oxygen (O_B) or the alcohol oxygen (O_A), along with the associated $g(R)$. The alcohol O_A hydrogen bonds to H_B when interacting with the BAS. The

https://doi.org/10.1021/jacs.5c09340
J. Am. Chem. Soc. 2025, 147, 26049−26059

$g(R)$ of H_B-O_B shows peak broadening from C_1 to C_4, with a tail stretching to longer distances as H_B is increasingly shared with the alcohol (Figure 6d-ii). In Figure 6d-iii, we see the H_B-O_A distance shortening with the carbon number. The relative position of H_B between O_B and O_A is the most clearly represented using the ΔR probability distribution shown in Figure 6d-iv; here, negative values of ΔR indicate that H_B is closer to O_B than to O_A and vice versa for positive values. For C_1, H_B is primarily on O_B with little probability of moving toward O_A. For C_2 and C_3, H_B shifts toward O_A but remains primarily on the side of O_B. For C_4, H_B is nearly equally shared between the two oxygens, forming a Zundel-like proton structure. Figure S7 shows that these changes are predominantly due to a shortening of the length of the O_A-H_B bond. This trend in ΔR follows the basicity of primary alcohols (see the pK_a in Table S1) and suggests a change in BAS interaction with increasing carbon number.

We expect the strength of the alcohol−OH interaction with the BAS to increase with increasing carbon number, which in turn reduces the acidity of the BAS−OH group.[43] Using DFT, we observe variations in the interaction of C_1-C_4 primary alcohols with the BAS. The trend in adsorption enthalpies is better captured by a polynomial fit than a linear one (Figure S8). Given the uniformity of the alkyl interaction with the zeolite framework (Figure 6c-ii,iii), the observed nonlinearity is attributed to the influence of the alkyl chain on the OH group, i.e., the increasing base strength of the OH group of primary alcohols. It is worth noting, however, that the degree of nonlinearity is very small, with the polynomial fit differing from the linear fit by an average of only 1.67 kJ mol^{-1}. Experimentally, this effect is not seen for primary alcohols. Yet, we do observe a decrease in the heat of adsorption of isomeric alcohols, which follows their basicity (see Supplementary Note 2). At present, the precise cause of this is unclear and is a subject for future investigation. We posit this to a pore confinement effect with changes in the strength of the O_A/H_B interaction being canceled out by increased repulsive interactions with the wall, conformational changes in the alcohol, and other convoluting factors. Similar effects were observed for branched alkanes, which showed significantly weaker interactions with the zeolite lattice compared to *n*-alkanes.[25] AIMD results indicate that variations in the BAS−OH binding strength are minimal and may be negligible, relative to these convoluting factors.

The presence of a BAS significantly complicates the computational modeling of interactions within the zeolite pores. While this study investigates a single BAS position, variations in BAS locations within the zeolite framework influence both acidity and adsorption behavior. Additionally, the orientation of adsorbed molecules plays a crucial role, as interactions along the "zigzag channels" or "straight channels" in H-MFI differ. These factors pose challenges for accurate modeling. Furthermore, nuclear quantum effects may influence the energetics of alcohol adsorption at the BAS, and prior studies have demonstrated their relevance at typical reaction temperatures.[44] Despite these complexities, the present agreement between theory and experiment suggests that the ensemble of these effects as measured experimentally yields an outcome comparable to the model employed here.

CONCLUSIONS

The present study provides a quantitative insight into the adsorption of C_1-C_4 alcohols and water on **MFI** and **Beta** frameworks by gravimetry, calorimetry, and theory. Correlations between the differential heat of adsorption of primary alcohols and the carbon number on siliceous and BAS containing frameworks reveal three distinct interactions between the alcohol molecules and the zeolite: (i) the interaction between the alkyl chain and the zeolite pore (approximately 10 kJ mol^{-1} per carbon atom), (ii) the interaction between the 1-alcohol−OH group and the zeolite pore (35 kJ mol^{-1} in the **MFI** framework and 30 kJ mol^{-1} in the **Beta** framework), and (iii) the interaction between the 1-alcohol−OH group and the BAS (37 kJ mol^{-1} in both **MFI** and **Beta** frameworks). Dipole−dipole interactions between the alkyl chain and the BAS, at only 10 kJ mol^{-1}, contribute to approximately one-third of the adsorption energy and can be neglected at the near-ambient temperatures in this study. The adsorption of water is nearly identical to the sorption enthalpies attributed to the OH group of the alcohols. The results demonstrate that hydrogen bonding to the surface is significantly stronger than the interaction between CH_x groups and the pore walls. The remarkable agreement between theory and experiment confirms that the interactions between each CH_x moiety and the zeolite framework remain invariant, with respect to the carbon number for C_1-C_4 alcohols. Similarly, the interaction between the alcohol hydroxyl group and the MFI zeolite framework also remains unchanged.

These findings provide fundamental insights into intermolecular forces, surface interactions, and confinement effects of zeolite-alcohol systems. Understanding how polar and nonpolar groups interact with zeolite pores will provide insights into catalytic reactions such as dehydration, dehydrogenation, and alkylation. This knowledge can be utilized to design more efficient catalytic processes in the petrochemical, pharmaceutical, and fine chemical industries.

MATERIALS AND METHODS

Materials. Si-MFI (Silicalite-1) and H-MFI (H-ZSM-5 with Si/Al = 45) with the **MFI** framework were obtained from *Clariant*. Si-BEA (siliceous) and H-BEA (Si/Al = 50) with the **Beta** framework were synthesized in the presence of fluoride following the procedure in a previous publication.[45] In brief, **Beta** zeolite was prepared by hydrothermal synthesis at 140 °C, with a gel composition of SiO_2:xAl_2O_3:(0.54 + 2x) TEAOH:(0.54 + 2x) HF:(7 + 2x) H_2O. Subsequently, the collected material was washed and filtrated with deionized water until the pH was neutral. To decompose the residues, e.g., organic cation (TEA^+), and remove fluoride anions, the dried material was calcined at 773 K for 2 h in synthetic air. Methanol (99.8%), ethanol (99.8%), 1-propanol (99.9%), 2-propanol (99.5%), 1-butanol (99.8%), 2-butanol (99.5%), and *iso*-butanol (≥99%) were purchased from *Sigma-Aldrich* and used as received.

Zeolite Characterization. The surface area and pore volume of the zeolite were determined by nitrogen physisorption. The N_2 adsorption isotherms were measured at 77 K using a *Porous Materials Inc.*. automatic *Sorptometer*. The zeolites were degassed in vacuum ($<10^{-3}$ mbar) at 623 K overnight before each measurement. Surface area was calculated by applying the Brunauer−Emmett−Teller theory, and the t-plot method was used to determine the micropore volumes.

Acid site concentration on H-MFI and H-BEA was determined by the IR spectroscopy of adsorbed pyridine on a *PerkinElmer 2000* spectrometer with a resolution of 4 cm^{-1}. The sample was shaped into a self-supporting wafer and activated under vacuum (10^{-6} mbar) at 723 K for 1 h. After cooling to 423 K, the sample was exposed and equilibrated with 0.1 mbar of pyridine vapor for 30 min with subsequent outgassing for 1 h. A spectrum of the chemisorbed pyridine was recorded thereafter. For quantification of acid site concentration, molar extinction coefficients of 0.73 and 0.96 cm μmol^{-1} were used for the band of pyridine on the Brønsted acid site

https://doi.org/10.1021/jacs.5c09340
J. Am. Chem. Soc. 2025, 147, 26049−26059

(at around 1545 cm^{-1}) and on the Lewis acid sites (at around 1450 cm^{-1}), respectively.

Adsorption Measurements. The adsorption of alcohols and water on all zeolite samples was measured gravimetrically and calorimetrically on a microbalance in a *Seteram TG-DSC 111* calorimeter connected to a high-vacuum system. After pretreatment of an approximately 20 mg sample at 723 K for 1 h under vacuum ($p < 10^{-4}$ mbar) with a heating rate of 10 K min^{-1}, the sample was cooled to 323 K. Afterward, the adsorbate was introduced into the system by controlled dosing. The adsorbed alcohol was determined in small pressure steps from 1×10^{-3} to 6−120 mbar (varying due to the differing vapor pressures of each alcohol) at 323 K. The adsorbed water was determined in small pressure steps from 1×10^{-3} to 20 mbar at 298 K. The adsorbate uptake was determined by the increase of sample weight, and the released heat was obtained by integration of the heat flux signal.

IR spectroscopy of alcohols in the gas phase and alcohols adsorbed on silica and Si-MFI was used to identify the interaction of the alcohol molecules and the interacting surface. All spectra were collected at 323 K on a Vertex 70 spectrometer from Bruker Optics at a resolution of 4 cm^{-1}. Sample wafers were loaded into a homemade IR cell connected to a vacuum system. It was first pretreated in vacuum ($p < 10^{-5}$ mbar) at 723 K for 1 h and cooled to 323 K. Alcohols were then introduced into the system by controlled dosing. The adsorbed alcohols were determined in small pressure steps from 1×10^{-2} to 10 mbar.

Computational Methods. We performed DFT-based AIMD simulations by modeling C_1−C_4 alcohol in **MFI** zeolite (same nomenclature as in the experiment: Si-MFI represents the zeolite without the BAS proton analogizing Silicalite-1, H-MFI represents the zeolite with the BAS proton analogizing H-ZSM-5). DFT calculations were performed under periodic boundary conditions with the GGA using the CP2K computational package.[46,47] The Perdew−Burke−Ernzerhoff exchange correlation functional[48] was used in conjunction with the dispersion corrections from the DFT-D3 method of Grimme et al.[49] Valence electrons were described using double-ζ quality basis sets[50] and core electrons with norm-conserving pseudopotentials.[51] Electrostatic terms were augmented with an auxiliary plane-wave basis set with a 400 Ry cutoff. The optimized cell was $20.022 \times 19.899 \times 13.383$ $Å^3$ for both Si-MFI and H-MFI. Based on the large size of this cell, Γ-point approximation was employed for Brillouin zone integration.

AIMD simulations were performed within the canonical NVT ensemble at 333 K with a time step of 0.5 fs and a Nosé−Hoover thermostat chain with a frequency of 4000 cm^{-1}. Each simulation trajectory contained a single alcohol molecule (C_1−C_4) within the zeolite framework. For H-MFI only, one BAS is present. To ascertain reliable statistical properties, we collected well-equilibrated data of 120−200 ps by discarding the initial 30−60 ps of data. The lowest energy structure of each system was determined through slow temperature annealing simulations followed by geometry optimization with TZV2PX basis sets. Structural characteristics were analyzed via plots of radial distribution functions, $g(R)$, which show distances between atomic pairs. The adsorption enthalpy was calculated by employing a QHA method, for which the vibrational density of states was calculated using the Fourier transform of the velocity autocorrelation function.[52−54]

■ ASSOCIATED CONTENT

Supporting Information

The Supporting Information is available free of charge at https://pubs.acs.org/doi/10.1021/jacs.5c09340.

Supplementary Note 1, additional characterization of C_1−C_4 primary alcohol adsorption; Supplementary Note 2, isomeric alcohol adsorption—influence of basicity; Supplementary Note 3, cluster formation of adsorbed alcohol molecules on BAS; Supplementary Note 4, additional figures and tables; and references (PDF)

■ AUTHOR INFORMATION

Corresponding Authors

Ruixue Zhao − *Department of Chemistry and Catalysis Research Center, Technical University of Munich, 85748 Garching, Germany;* orcid.org/0000-0001-7251-5423; Email: ruixue.zhao@tum.de

Sungmin Kim − *Institute for Integrated Catalysis, Pacific Northwest National Laboratory, Richland, Washington 99352, United States;* orcid.org/0000-0001-6602-1320; Email: sungmin.kim@pnnl.gov

Mal-Soon Lee − *Institute for Integrated Catalysis, Pacific Northwest National Laboratory, Richland, Washington 99352, United States;* orcid.org/0000-0001-6851-177X; Email: malsoon.lee@pnnl.gov

Johannes A. Lercher − *Department of Chemistry and Catalysis Research Center, Technical University of Munich, 85748 Garching, Germany; Institute for Integrated Catalysis, Pacific Northwest National Laboratory, Richland, Washington 99352, United States;* orcid.org/0000-0002-2495-1404; Email: johannes.lercher@ch.tum.de

Authors

Benjamin A. Jackson − *Institute for Integrated Catalysis, Pacific Northwest National Laboratory, Richland, Washington 99352, United States;* orcid.org/0000-0001-6205-8951

Fuli Deng − *Department of Chemistry and Catalysis Research Center, Technical University of Munich, 85748 Garching, Germany*

Xiaomai Chen − *Department of Chemistry and Catalysis Research Center, Technical University of Munich, 85748 Garching, Germany*

Cong Zhou − *Institute for Integrated Catalysis, Pacific Northwest National Laboratory, Richland, Washington 99352, United States*

Konstantin Khivantsev − *Institute for Integrated Catalysis, Pacific Northwest National Laboratory, Richland, Washington 99352, United States;* orcid.org/0000-0002-4810-586X

Yue Liu − *Department of Chemistry and Catalysis Research Center, Technical University of Munich, 85748 Garching, Germany; Shanghai Key Laboratory of Green Chemistry and Chemical Processes, School of Chemistry and Molecular Engineering, East China Normal University, Shanghai 200062, PR China;* orcid.org/0000-0001-8939-0233

Vassiliki-Alexandra Glezakou − *Institute for Integrated Catalysis, Pacific Northwest National Laboratory, Richland, Washington 99352, United States;* Present Address: Chemical Science Division, Oak Ridge National Laboratory, Oak Ridge, Tennessee 37830, United States; orcid.org/0000-0001-6028-7021

Roger Rousseau − *Institute for Integrated Catalysis, Pacific Northwest National Laboratory, Richland, Washington 99352, United States;* Present Address: Chemical Science Division, Oak Ridge National Laboratory, Oak Ridge, Tennessee 37830, United States; orcid.org/0000-0003-1947-0478

Complete contact information is available at: https://pubs.acs.org/10.1021/jacs.5c09340

Notes

The authors declare no competing financial interest.

https://doi.org/10.1021/jacs.5c09340
J. Am. Chem. Soc. 2025, 147, 26049−26059

■ ACKNOWLEDGMENTS

This work was supported by the U.S. Department of Energy (DOE), Office of Science, Office of Basic Energy Sciences (BES), Division of Chemical Sciences, Geosciences and Biosciences (Advancing key catalytic reaction steps for achieving carbon neutrality, FWP 47319). V.-A.G. and R.R. acknowledge partial support from the US DOE BES at Oak Ridge National Laboratory (ORNL). ORNL is operated by UT-Battelle under contract no. DE-AC05-00OR22725 for the U.S. Department of Energy.

■ REFERENCES

(1) Kessel, A.; Ben-Tal, N. *Introduction to proteins: structure, function, and motion*; Chapman and Hall/CRC, 2018.
(2) Raynal, M.; Ballester, P.; Vidal-Ferran, A.; van Leeuwen, P. W. Supramolecular catalysis. Part 1: non-covalent interactions as a tool for building and modifying homogeneous catalysts. *Chem. Soc. Rev.* **2014**, *43* (5), 1660−1733.
(3) Gounder, R.; Iglesia, E. Catalytic consequences of spatial constraints and acid site location for monomolecular alkane activation on zeolites. *J. Am. Chem. Soc.* **2009**, *131* (5), 1958−1971.
(4) Schallmoser, S.; Haller, G. L.; Sanchez-Sanchez, M.; Lercher, J. A. Role of spatial constraints of Brønsted acid sites for adsorption and surface reactions of linear pentenes. *J. Am. Chem. Soc.* **2017**, *139* (25), 8646−8652.
(5) Göltl, F.; Hafner, J. Modelling the adsorption of short alkanes in protonated chabazite: The impact of dispersion forces and temperature. *Microporous and mesoporous materials* **2013**, *166*, 176−184.
(6) Göltl, F.; Hafner, J. Alkane adsorption in Na-exchanged chabazite: The influence of dispersion forces. *J. Chem. Phys.* **2011**, *134* (6), No. 064102.
(7) Eder, F.; Lercher, J. A. Alkane sorption in molecular sieves: The contribution of ordering, intermolecular interactions, and sorption on Brønsted acid sites. *Zeolites* **1997**, *18* (1), 75−81.
(8) Barrer, R. M.; Sutherland, J. Inclusion complexes of faujasite with paraffins and permanent gases. *Proc. R. Soc. Lond. Ser. A. Math. Phys. Sci.* **1956**, *237* (1211), 439−463.
(9) Narbeshuber, T. F.; Vinek, H.; Lercher, J. A. Monomolecular Conversion of Light Alkanes over H-ZSM-5. *J. Catal.* **1995**, *157* (2), 388−395.
(10) Li, H.; Kadam, S. A.; Vimont, A.; Wormsbecher, R. F.; Travert, A. Monomolecular Cracking Rates of Light Alkanes over Zeolites Determined by IR Operando Spectroscopy. *ACS Catal.* **2016**, *6* (7), 4536−4548.
(11) De Moor, B. A.; Reyniers, M.-F. o.; Gobin, O. C.; Lercher, J. A.; Marin, G. B. Adsorption of C_2−C_8 n-Alkanes in Zeolites. *J. Phys. Chem. C* **2011**, *115* (4), 1204−1219.
(12) Swisher, J. A.; Hansen, N.; Maesen, T.; Keil, F. J.; Smit, B.; Bell, A. T. Theoretical Simulation of n-Alkane Cracking on Zeolites. *J. Phys. Chem. C* **2010**, *114* (22), 10229−10239.
(13) Tranca, D. C.; Hansen, N.; Swisher, J. A.; Smit, B.; Keil, F. J. Combined Density Functional Theory and Monte Carlo Analysis of Monomolecular Cracking of Light Alkanes Over H-ZSM-5. *J. Phys. Chem. C* **2012**, *116* (44), 23408−23417.
(14) Janda, A.; Vlaisavljevich, B.; Lin, L.-C.; Mallikarjun Sharada, S.; Smit, B.; Head-Gordon, M.; Bell, A. T. Adsorption Thermodynamics and Intrinsic Activation Parameters for Monomolecular Cracking of n-Alkanes on Brønsted Acid Sites in Zeolites. *J. Phys. Chem. C* **2015**, *119* (19), 10427−10438.
(15) Berger, F.; Rybicki, M.; Sauer, J. Molecular Dynamics with Chemical Accuracy—Alkane Adsorption in Acidic Zeolites. *ACS Catal.* **2023**, *13* (3), 2011−2024.
(16) Piccini, G.; Alessio, M.; Sauer, J.; Zhi, Y.; Liu, Y.; Kolvenbach, R.; Jentys, A.; Lercher, J. A. Accurate Adsorption Thermodynamics of Small Alkanes in Zeolites. Ab initio Theory and Experiment for H-Chabazite. *J. Phys. Chem. C* **2015**, *119* (11), 6128−6137.
(17) Barrer, R. M.; Davies, J. Sorption in decationated zeolites II. Simple paraffins in H-forms of chabazite and zeolite L. *Proc. R. Soc. Lond. A. Math. Phys. Sci.* **1971**, *322* (1548), 1−19.
(18) Stach, H.; Lohse, U.; Thamm, H.; Schirmer, W. Adsorption equilibria of hydrocarbons on highly dealuminated zeolites. *Zeolites* **1986**, *6* (2), 74−90.
(19) Savitz, S.; Siperstein, F.; Gorte, R. J.; Myers, A. L. Calorimetric Study of Adsorption of Alkanes in High-Silica Zeolites. *J. Phys. Chem. B* **1998**, *102* (35), 6865−6872.
(20) Krishna, R.; Smit, B.; Calero, S. Entropy effects during sorption of alkanes in zeolites. *Chem. Soc. Rev.* **2002**, *31* (3), 185−194.
(21) Arik, I. C.; Denayer, J. F.; Baron, G. V. High-temperature adsorption of n-alkanes on ZSM-5 zeolites: influence of the Si/Al ratio and the synthesis method on the low-coverage adsorption properties. *Microporous and mesoporous materials* **2003**, *60* (1−3), 111−124.
(22) Eder, F.; Stockenhuber, M.; Lercher, J. Brønsted acid site and pore controlled siting of alkane sorption in acidic molecular sieves. *J. Phys. Chem. B* **1997**, *101* (27), 5414−5419.
(23) Calero, S.; Dubbeldam, D.; Krishna, R.; Smit, B.; Vlugt, T. J. H.; Denayer, J. F. M.; Martens, J. A.; Maesen, T. L. M. Understanding the Role of Sodium during Adsorption: A Force Field for Alkanes in Sodium-Exchanged Faujasites. *J. Am. Chem. Soc.* **2004**, *126* (36), 11377−11386.
(24) Dunne, J. A.; Rao, M.; Sircar, S.; Gorte, R. J.; Myers, A. L. Calorimetric Heats of Adsorption and Adsorption Isotherms. 2. O_2, N_2, Ar, CO_2, CH_4, C_2H_6, and SF_6 on NaX, H-ZSM-5, and Na-ZSM-5 Zeolites. *Langmuir* **1996**, *12* (24), 5896−5904.
(25) Sievers, C.; Onda, A.; Olindo, R.; Lercher, J. A. Adsorption and Polarization of Branched Alkanes on H−LaX. *J. Phys. Chem. C* **2007**, *111* (14), 5454−5464.
(26) Mei, D.; Lercher, J. A. Mechanistic insights into aqueous phase propanol dehydration in H-ZSM-5 zeolite. *AIChE J.* **2017**, *63* (1), 172−184.
(27) Humplik, T.; Raj, R.; Maroo, S. C.; Laoui, T.; Wang, E. N. Effect of Hydrophilic Defects on Water Transport in MFI Zeolites. *Langmuir* **2014**, *30* (22), 6446−6453.
(28) Eckstein, S.; Hintermeier, P. H.; Zhao, R.; Baráth, E.; Shi, H.; Liu, Y.; Lercher, J. A. Influence of Hydronium Ions in Zeolites on Sorption. *Angew. Chem., Int. Ed.* **2019**, *58* (11), 3450−3455.
(29) Karbowiak, T.; Saada, M.-A.; Rigolet, S.; Ballandras, A.; Weber, G.; Bezverkhyy, I.; Soulard, M.; Patarin, J.; Bellat, J.-P. New insights in the formation of silanol defects in silicalite-1 by water intrusion under high pressure. *Phys. Chem. Chem. Phys.* **2010**, *12* (37), 11454−11466.
(30) Wang, M.; Jaegers, N. R.; Lee, M.-S.; Wan, C.; Hu, J. Z.; Shi, H.; Mei, D.; Burton, S. D.; Camaioni, D. M.; Gutiérrez, O. Y.; et al. Genesis and Stability of Hydronium Ions in Zeolite Channels. *J. Am. Chem. Soc.* **2019**, *141* (8), 3444−3455.
(31) Hack, J. H.; Ma, X.; Chen, Y.; Dombrowski, J. P.; Lewis, N. H. C.; Li, C.; Kung, H. H.; Voth, G. A.; Tokmakoff, A. Proton Dissociation and Delocalization under Stepwise Hydration of Zeolite HZSM-5. *J. Phys. Chem. C* **2023**, *127* (32), 16175−16186.
(32) Liu, Q.; Pfriem, N.; Cheng, G.; Baráth, E.; Liu, Y.; Lercher, J. A. Maximum Impact of Ionic Strength on Acid-Catalyzed Reaction Rates Induced by a Zeolite Microporous Environment. *Angew. Chem., Int. Ed.* **2023**, *62* (3), No. e202208693.
(33) Bregante, D. T.; Chan, M. C.; Tan, J. Z.; Ayla, E. Z.; Nicholas, C. P.; Shukla, D.; Flaherty, D. W. The shape of water in zeolites and its impact on epoxidation catalysis. *Nature Catalysis* **2021**, *4* (9), 797−808.
(34) Pfriem, N.; Hintermeier, P. H.; Eckstein, S.; Kim, S.; Liu, Q.; Shi, H.; Milakovic, L.; Liu, Y.; Haller, G. L.; Baráth, E. Role of the ionic environment in enhancing the activity of reacting molecules in zeolite pores. *Science* **2021**, *372* (6545), 952−957.
(35) Kim, S.; Chen, F.; Camaioni, D. M.; Derewinski, M. A.; Gutiérrez, O. Y.; Liu, Y.; Lercher, J. A. Confined Ionic Environments Tailoring the Reactivity of Molecules in the Micropores of BEA-Type Zeolite. *J. Am. Chem. Soc.* **2024**, *146* (26), 17847−17853.

https://doi.org/10.1021/jacs.5c09340
J. Am. Chem. Soc. 2025, 147, 26049−26059

(36) Natal-Santiago, M.; Dumesic, J. Microcalorimetric, FTIR, and DFT studies of the adsorption of methanol, ethanol, and 2, 2, 2-trifluoroethanol on silica. *Journal of catalysis* **1998**, *175* (2), 252−268.
(37) Azrak, R. G.; Angell, C. Study of alcohol-silica surface reactions via infrared spectroscopy. *J. Phys. Chem.* **1973**, *77* (26), 3048−3052.
(38) Van Ness, H. C.; Van Winkle, J.; Richtol, H. H.; Hollinger, H. B. Infrared spectra and the thermodynamics of alcohol-hydrocarbon systems. *J. Phys. Chem.* **1967**, *71* (5), 1483−1494.
(39) Suresh, S.; Naik, V. Hydrogen bond thermodynamic properties of water from dielectric constant data. *J. Chem. Phys.* **2000**, *113* (21), 9727−9732.
(40) Curtiss, L. A.; Jones, C.; Trucks, G. W.; Raghavachari, K.; Pople, J. A. Gaussian-1 theory of molecular energies for second-row compounds. *J. Chem. Phys.* **1990**, *93* (4), 2537−2545.
(41) Pople, J. A.; Head-Gordon, M.; Fox, D. J.; Raghavachari, K.; Curtiss, L. A. Gaussian-1 theory: A general procedure for prediction of molecular energies. *J. Chem. Phys.* **1989**, *90* (10), 5622−5629.
(42) Galimberti, D. R.; Sauer, J. Chemically Accurate Vibrational Free Energies of Adsorption from Density Functional Theory Molecular Dynamics: Alkanes in Zeolites. *J. Chem. Theory Comput.* **2021**, *17* (9), 5849−5862.
(43) Graham Solomons, T. W.; Fryhle, C. B.; Snyder, S. A. *Organic Chemistry*; John Wiley & Sons, Inc., 2016.
(44) Bocus, M.; Goeminne, R.; Lamaire, A.; Cools-Ceuppens, M.; Verstraelen, T.; Van Speybroeck, V. Nuclear quantum effects on zeolite proton hopping kinetics explored with machine learning potentials and path integral molecular dynamics. *Nat. Commun.* **2023**, *14* (1), 1008.
(45) Prodinger, S.; Shi, H.; Wang, H.; Derewinski, M. A.; Lercher, J. A. Impact of structural defects and hydronium ion concentration on the stability of zeolite BEA in aqueous phase. *Applied Catalysis B: Environmental* **2018**, *237*, 996−1002.
(46) Kühne, T. D.; Iannuzzi, M.; Del Ben, M.; Rybkin, V. V.; Seewald, P.; Stein, F.; Laino, T.; Khaliullin, R. Z.; Schütt, O.; Schiffmann, F.; et al. CP2K: An electronic structure and molecular dynamics software package - Quickstep: Efficient and accurate electronic structure calculations. *J. Chem. Phys.* **2020**, *152* (19), 194103.
(47) VandeVondele, J.; Krack, M.; Mohamed, F.; Parrinello, M.; Chassaing, T.; Hutter, J. Quickstep: Fast and accurate density functional calculations using a mixed Gaussian and plane waves approach. *Comput. Phys. Commun.* **2005**, *167* (2), 103−128.
(48) Perdew, J. P.; Burke, K.; Ernzerhof, M. Generalized gradient approximation made simple. *Physical review letters* **1996**, *77* (18), 3865.
(49) Grimme, S.; Antony, J.; Ehrlich, S.; Krieg, H. A consistent and accurate ab initio parametrization of density functional dispersion correction (DFT-D) for the 94 elements H-Pu. *J. Chem. Phys.* **2010**, *132* (15), 154104.
(50) VandeVondele, J.; Hutter, J. Gaussian basis sets for accurate calculations on molecular systems in gas and condensed phases. *J. Chem. Phys.* **2007**, *127* (11), 114105.
(51) Goedecker, S.; Teter, M.; Hutter, J. Separable dual-space Gaussian pseudopotentials. *Phys. Rev. B* **1996**, *54* (3), 1703.
(52) Marin, G. B.; Glezakou, V.-A.; Rousseau, R.; Lercher, J. A.; Alexopoulos, K.; Lee, M.-S.; Liu, Y.; Zhi, Y.; Liu, Y.; Reyniers, M.-F. Anharmonicity and confinement in zeolites: structure, spectroscopy, and adsorption free energy of ethanol in H-ZSM-5. *J. Phys. Chem. C* **2016**, *120* (13), 7172−7182.
(53) Yuk, S. F.; Lee, M.-S.; Collinge, G.; Zhang, J.; Padmaperuma, A. B.; Li, Z.; Polo-Garzon, F.; Wu, Z.; Glezakou, V.-A.; Rousseau, R. Mechanistic understanding of catalytic conversion of ethanol to 1-butene over 2D-Pillared MFI zeolite. *J. Phys. Chem. C* **2020**, *124* (52), 28437−28447.
(54) De Sousa, R. L.; Leite Alves, H. W. Ab initio calculation of the dynamical properties of PPP and PPV. *Braz. J. Phys.* **2005**, *36*, 501−504.

https://doi.org/10.1021/jacs.5c09340
J. Am. Chem. Soc. 2025, 147, 26049−26059